
Article:

Zhai, X, Li, Z, Zhang, J et al. (9 more authors) (2018) Natural Biomaterial-Based Edible and pH-Sensitive Films Combined with Electrochemical Writing for Intelligent Food Packaging. Journal of Agricultural and Food Chemistry, 66 (48). pp. 12836-12846. ISSN 0021-8561

https://doi.org/10.1021/acs.jafc.8b04932

Natural biomaterial-based edible and pH-sensitive films combined with electrochemical writing for intelligent food packaging

Xiaodong Zhai[†, ‖], Zhihua Li[†, ‖], Junjun Zhang[†, ‖], Jiyong Shi[†, ‖], Xiaobo Zou[*, †, ‖], Xiaowei Huang[†, ‖], Yue Sun[†, ‖], Wen Zhang[†, ‖], Zhikun Yang[†, ‖], Mel Holmes[‡, ‖], Yunyun Gong[‡, ‖], Povey, Megan J[‡, ‖]

[†]Agricultural Product Processing and Storage Lab, School of Food and Biological Engineering, Jiangsu University, Zhenjiang, Jiangsu 212013, China

[‡]School of Food Science and Nutrition, the University of Leeds, Leeds LS2 9JT, United Kingdom

[‖]China-UK joint laboratory for nondestructive detection of agro-products, Jiangsu University, Zhenjiang, Jiangsu 212013, China

[*] Corresponding author. Tel.: +86 511 88780174; fax: +86 511 88780201; Email: zou_xiaobo@ujs.edu.cn

ABSTRACT

An edible and pH-sensitive film combined with electrochemical writing was developed using gelatin, gellan gum and red radish anthocyanin extract for intelligent food packaging applications. The composite film displays orange red-to-yellow color change over the pH range 2-12. The tensile strength, ductility, and barrier response of the films to UV light and oxygen improved with the increase of red radish anthocyanin concentration. Multicolor patterns were successfully drawn on the film using an electrochemical writing method. The composite films acted as gas sensors which presented visible color changes in the presence of milk and fish spoilage, while the written patterns were well preserved. Accordingly, this composite film with written patterns could be an easy-to-use indicator with great potential for monitoring food spoilage as part of an intelligent packaging system.

KEYWORDS: intelligent food packaging; gelatin; gellan gum; red radish anthocyanins; electrochemical writing; film

1. INTRODUCTION

Intelligent food packaging has received great interests in the last decades, because of their potential for monitoring the condition of packaged foods or the surrounding environment.[1] Generally, intelligent food packaging systems can be realized by three main technologies, namely sensors, indicators and data carriers.[2] Among these systems, indicators (e.g. freshness indicators, time-temperature indicators and gas indicators) which could provide qualitative or semi-quantitative information by means of a color change have been widely studied since they are easy to fabricate and can be read by naked eye.

In recent years, many pH–sensitive indicators have been developed to monitor food quality. This was because various non-neutral volatile gases, such as amines, hydrogen sulfide and carbon dioxide, can be generated from foods during spoilage. When these volatile gases diffused to the headspace of the packages, they could react with the pH-sensitive indicators and thus make color changes of the indicators. Generally, the pH-sensitive materials were composed of pH dyes and a solid matrix to immobilize the pH dyes.[3, 4]. Considering that traditional synthetic pH dyes with potential harmful effects to human beings are not ideal for food packaging,[5] more attentions have recently been paid to natural and safe pigments, such as anthocyanins [6-14] and curcumin.[15-18] In addition, due to the public concern over environmental problems caused by plastics, there is a greater demand for packaging materials made by eco-friendly biopolymers with good film-forming properties, such as starch, chitosan, gums, alginate, agar, gelatin and so forth.

Red radish (Raphanus sativus L.) (RR) is a anthocyanins-rich vegetable,[19] in which anthocyanins mainly exist at acylated structures.[20] Anthocyanins extracted from red radish are widely used as natural food-coloring agents because of their high stability and their orange-red color similar to that of synthetic Food Red No. 40.[20, 21] As red radish is also widespread and low cost, the red radish anthocyanins (RRA) could be a good resource of pH-sensitive pigments. The solid matrix used to immobilize anthocyanins is also of great importance. Gelatin is a denatured protein from the triple helix of collagen. It is accepted as “Generally Recognized as Safe’’ (GRAS) substance in the area of food additives by the US Food and Drug Administration (FDA).[22] Gelatin is also considered as a promising natural polymer for packaging applications because of its renewability, biodegradability and film-forming property.[23] Particularly, gelatin films possess good oxygen barrier property.[22] This may be used to protect packaged foods from being oxidized to some extent and thus improve their shelf life. However, poor mechanical properties (such as frangibility) have been described as one of the disadvantages of gelatin films.[24] To compensate this shortcoming, gelatin is generally cross-linked and/or combined with other polymers, such as sodium alginate [25] and chitosan.[26] Gellan gum, a linear negatively charged exopolysaccharide, is biodegradable and non-toxic in nature. Four repeating carbohydrates are present in the main chain of gellan gum, which includes two d-glucose carbohydrates, one L-rhamnose, and one D-glucuronic acid.[27] It has received both US FDA and EU (E418) approval for application mainly as a multi-functional gelling, stabilizing and suspending agent in a variety of foods and personal care products.[28] Importantly, it was found that the mechanical properties of gelatin film could be significantly improved by gellan gum.[29] Furthermore, a recent study showed that gellan gum could enhance the thermal stability of anthocyanins.[30] Hence, the gelatin/gellan gum blend could be a good film-forming agent to immobilize anthocyanins.

Most food packaging materials are printed in order to provide information about the packaged foods and many inks are still mainly derived from petrochemical feedstock, which brings significant environment and sustainability problems to modern society.[31] In addition, the migration of unsafe printing inks from packaging to food can be a risk for consumers health.[32] To solve these problems, new inks such as edible inks and new techniques for printing are very desirable.[33] Recently, Wu, et al. [34] successfully printed on polysaccharide film by an electrochemical method based on the pH response color change of anthocyanins. As anthocyanins are safe and biodegradable, this electrochemical writing can be regarded as a green printing method. However, the related work of electrochemical writing on edible films is still limited.

In this study, we aimed to develop a new pH-sensitive and edible film by using RRA as the pH-sensitive pigment and gelatin/gellan gum blend as the film-forming agent, respectively. The fundamental properties of films, such as microstructure, mechanical properties and gas permeability properties were first investigated. Then, multicolor patterns were written on this polysaccharide/protein composite film by using an electrochemical writing method. Finally, the film combined with written patterns was used to indicate milk and fish quality.

2. MATERIALS AND METHODS

2.1. Materials and Reagents. Fresh red radish (cultivar ‘Xinlimei’) and live black carp were purchased from local market, and pasteurized milk was bought from a local cattle farm (Zhenjiang, China). Gelatin (type B, pig skin) was purchased from Sigma-Aldrich Inc. (St. Louis, MO, USA). Low-acyl gellan gum was bought from Dancheng Caixin sugar industry Co., ltd. (Dancheng, China). Other chemical agents, such as ethyl alcohol, calcium chloride, acetic acid, ammonium hydroxide, acetonitrile and formic acid were bought from Sinopharm Chemical Reagent Co., Ltd (Shanghai, China).

2.2. Extraction of anthocyanins from red radish. Fresh red radishes were peeled, cut into pieces and dried at 65 °C under vacuum. Then, the dried red radishes were crushed into powder and transferred to 80% ethanol aqueous solution with a solid-liquid ratio of 1:10. After stirring at 35 °C for 6 h, supernatant of the solution was collected through filtration using a 25-μm filter paper. Ethanol in the supernatant was removed with a vacuum rotary evaporator at 45 °C in dark. Finally, the concentrated RRA extract solution was freeze-dried under vacuum and the obtained RRA extract powder was stored at 4 °C in a brown bottle filled with nitrogen.

The anthocyanins content in lyophilized RRA extract powder was measured by the pH differential method.[35] Absorbance of sample at 520 and 700 nm was measured using a UV-Vis spectrophotometry (Agilent CARY 100, Varian Corporation, USA). The anthocyanin content was expressed in mg/g.

2.3. Preparation of films. Firstly, 100 mL aqueous dispersion containing 3 g of gelatin (G) and 1 g of gellan gum (GG) was heated at 85 ℃ in a water bath and stirred with a magnetic stirrer for 0.5 h to form a clear solution. Under this constant temperature, 30 mg of $CaCl_2 \cdot 2H_2O$ was added into the solution with continuous stirring. Based on the calculated anthocyanins content (303.42 ± 7.82 mg/g) (refer to section 2.3), RRA extract powder was then added to the solution to obtain an anthocyanin contents of 5 mg/100 mL, 10 mg/100 mL, 15 mg/100 mL and 20 mg/100 mL, expressed as RRA5, RRA10, RRA15 and RRA20. A control solution containing gelatin, gellan gum and $CaCl_2 \cdot 2H_2O$ was also prepared. After degassing with a sonicator at 85 ℃, 12 g of the film-forming solution was immediately poured into a clean and smooth plastic Petri dish with a 9 cm diameter. Then, firm hydrogels were formed after the solutions were cooled down. The hydrogels were dried to films by putting the Petri dishes on a horizontal platform in an oven at 45 ℃ for 2 h. After that, the film was peeled from the Petri dishes and stored in an incubator at 4 ℃ with 75% RH for further use.

In order to prepare films with electrochemical writing, the above-mentioned hydrogels containing RRA were firstly taken out from the Petri dish before drying. The hydrogel was contacted with a platinum (Pt) plate connected to the cathode of an electrochemical analyzer (CHI660E, CH Instruments Co., Shanghai, China). Then, a Pt needle (diameter 0.5 mm) connected to the anode of the electrochemical analyzer touched the upper surface of the hydrogel. Under a constant current, hydrogen ions were produced around the platinum needle and thus induced an orange red color of RRA. On the contrary, when the Pt plate was connected to the anode of the electrochemical analyzer and the Pt needle was connected to the cathode of the electrochemical analyzer, hydroxyl ions were produced around the Pt needle and thus induced a green color of RRA. The movement of the platinum needle was procedurally controlled by a mechanical arm with a step precision of 0.1 μm (DOBOT M1, Shenzhen Yuejiang Technology Co., Ltd, China). The hydrogel was immediately dried in a vacuum-drying oven at 70 °C to form a film and the film was stored at 4 °C with 75% RH before use.

2.4. Characterization of the films

2.4.1. Color response to pH variation. UV-vis spectra of films were measured using a UV-vis spectrophotometer (Agilent CARY 100, Varian Corporation, USA). Firstly, pH buffer solutions (pH 2-12) were prepared by using 0.2 M disodium hydrogen phosphate, 0.2 M citric acid and 0.2 M sodium hydroxide solutions with different proportions. Then, films were cut into squares (1 cm × 1 cm) and immersed in the buffer solutions for 5 min. The spectra of the films in the range of 400-800 nm were obtained using air as the blank.

2.4.2. Microstructure observation. The micrographs of the films were recorded by a field emission scanning electron microscope (FE-SEM) (S-4800, Hitachi High Technologies Corporation, Japan). The films were first freeze fractured by liquid nitrogen before measurement. Samples were attached to double-sided adhesive tape and mounted on the specimen holder, then sputtered and coated with gold under vacuum.

2.4.3. Mechanical properties. Tensile strength (TS) and elongation-at-break (EB) of the films were measured with an Instron Universal Testing Machine (Model 4500, Instron Corporation, Canton, MA, USA) using a modified ASTM D882-00 (ASTM, 2000b) procedure. Samples were conditioned at 25 °C and 50 ± 3% RH in a desiccator containing magnesium nitrate saturated solution for 2 d prior to analysis. Each film was cut in rectangular strips with 60 mm length and 20 mm width. The initial grip separation and crosshead speed were set at 40 mm and 0.6 mm/s respectively. The TS and EB were calculated as the equation (1) and (2), respectively. Measurements represent an average of six samples.

$$\mathrm{TS} = \mathrm{F}_{\max} / \mathrm{S} \tag{1}$$

$$E(\%) = 100 \times \Delta l / l_0 \quad (2)$$

where TS was the tensile strength (MPa); F_{max} was the maximun load (N); S was the the initial cross-sectional area of the film sample (mm2); E was the elongation-at-break; *Δl* was the extension of the film (mm) and l_0 was the intial test length of the film (40 mm).

2.4.4. Transparency measurement. The optical transmittance of GGG and GGG-RRA films (2 cm × 1 cm) were measured in the range of 200–800 nm with air as the blank by using the UV–vis spectrophotometer.

2.4.5. Water vapor permeability. Water vapor permeability (WVP) of films was determined gravimetrically using a standard test method (ASTM E96-05). The film samples that had previously equilibrated at 50% RH for 48 h were sealed on glass cups containing dried silica gel (0% RH). The cups were then placed in desiccators containing saturated $Mg(NO3)_2$ solution (50% RH) at 25 °C. The cups were weighed at 1-h interval until a steady state was reached. The water vapor transmission rate (WVTR) of a film was determined from the slope of the regression analysis of weight gain of moisture (Δm) that transferred through a film area (A) during a definite time (t), as shown in equation (3). Then, the WVP of the film was calculated based on the WVTR, as shown in equation (4). Measurements represent an average of six samples.

$$\mathrm{WVTR} = \Delta m / (A \times t) \quad (3)$$

$$\mathrm{WVP} = \mathrm{WVTR} \times x / \Delta P \quad (4)$$

where Δm is the weight gain of the cup (g); x is the film thickness (m); A is the exposed area (m^2); ΔP is the partial water vapor pressure difference across the film (1583.7 Pa at 25℃); t is the time (h).

2.4.6. Oxygen permeability. Oxygen permeability (OP) of the film was estimated at 25 ℃ and 50% RH with an automated oxygen permeability testing machine (GTR-7001, SYSTESTER, China) following the standard method (ASTM D3985-05, 2005). Film was placed on a stainless-steel mask with an open testing area of 48 cm^2. Oxygen and nitrogen were respectively flowed on each side of the films. Oxygen transmission rate (OTR) was measured and OP was calculated according to equation (5). Measurements represent an average of six samples.

$$\mathrm{OP} = \mathrm{OTR} \times x / \Delta \mathrm{P} \tag{5}$$

where OTR is the oxygen transmission rate ($cm^3 \cdot m^{-2} \cdot d^{-1}$); x is the film thickness (m); ΔP is the partial pressure of oxygen (1.013×10^5 Pa at 25 °C).

2.4.7. Color stability. The colorimetric films were stored in incubators at 4℃ and 25℃ with 75% RH under fluorescent lights. The images of the colorimetric films were captured every day for two weeks by an optical scanner (Scanjet G4050, HP) and analyzed by a user program in Matlab R2012a (Matworks Inc., Natick, MA, USA). The stability of the colorimetric films was defined as the relative colour change, according to our previous study: [36]

$$\Delta \mathrm{R} = \left| \mathrm{R}_0 - \mathrm{R}_1 \right| \tag{6}$$

$$\Delta G = \left| G_0 - G_1 \right| \tag{7}$$

$$\Delta B = \left| B_0 - B_1 \right| \tag{8}$$

$$S = \left(\Delta R + \Delta G + \Delta B \right) / (R_0 + G_0 + B_0) \times 100\% \tag{9}$$

where R_0, G_0, B_0 were the initial gray values of the red, green and blue, R_1, G_1, B_1 were the gray values of the red, green and blue after storage. S was the relative color change of R, G and B values.

2.4.8. Color response to basic and acid gases. Response of the colorimetric films toward volatile ammonia in term of their color changes was performed using absorbance measurements. The colorimetric films were hang up in an Erlenmeyer flask (500 mL) at 1 cm above the ammonia solution (80 mL, 8 mM) at 25℃.

2.5. Application of films in monitoring food quality

2.5.1. Milk spoilage trial. 20 mL of pasteurized fresh milk was poured into an unused plastic Petri dish (diameter 90 mm) with a lid. In the middle of the lid, a square hole was cut using a knife. Then the film was fixed on the lid to cover the hole. The Petri dish was sealed with Vaseline and placed in an incubator at 25 ℃ with 75% RH. During milk spoilage, volatile gases were generated from the milk and diffuse through the film, making a color change of the film. The images of the film were captured using the optical scanner. The acidity of milk was measured by acid-base titration method according to a previous literature.[37]

2.5.2. Fish spoilage trial. Fresh black carp (Mylopharyngodon piceus) was cut into strips after removing its innards, head, tail and scales. Like the milk spoilage trail, 25 g of black carp was put into the plastic Petri dish and the film was fixed on the lid to cover the hole. The Petri dish was placed in an incubator at 4 ℃ with 75% RH. The total volatile basic nitrogen (TVB-N) content was measured according to a previous literature.[38]

3. RESULTS AND DISCUSSION

3.1. Color and UV-vis spectra of RRA and GGG-RRA film. In this study, RRA was used as the pH-sensitive pigment to develop packaging films, so the color response of RRA and GGG-RRA film to pH variation was firstly investigated. Fig. 1A shows that RRA solutions changed from orange red to yellow when pH increased from 2 to 12. In detail, RRA solution turned from deep orange red to light orange over the pH range of 2-7. At weak basic conditions, the color became purple (pH 8-9). Then, the color changed to yellow green (pH 10) and finally to yellow (pH 10-12). Corresponding to color changes in RRA solutions, the maximum absorption peak presented red-shifts. As shown in Fig. 1B, the maximum absorption peak obtained at pH 2 was around 510 nm, which gradually shifted to 520 nm when the pH increased to 6. Meanwhile, the maximum absorption values decreased. As the pH increased over 7, the maximum absorption peak shifted to approximately 580 nm. At the same time, the absorption values gradually increased when pH increased from 7 to 10 and then decreased when pH increased from 10 to 12. The absorbance ratio at 580 nm versus 510 nm (A_{580}/A_{510}) indicates the increase of green intensity compared to red. The calibration curve (Fig. 1B inset) showed that values of A_{580}/A_{510} in PSPE solution increased and then decreased over the range of pH 2-9. An exponential calibration curve was established between the pH in the range of 2-9 and

A_{580}/A_{510} of the RRA solution, as formula (10), where x and y were the pH and A_{580}/A_{510}, respectively.

$$y = 0.1399e^{0.2745x}, R^2 = 0.9823 \qquad (10)$$

The GGG film containing RRA showed similar color (Fig. 1C) and spectra (Fig. 1D) changes with RRA in response to pH variation. An exponential calibration curve was also established between the pH in the range of 2-9 and A_{580}/A_{510} of the GGG-RRA film (Fig. 1D inset), according to the formula (11), where x and y were the pH and A_{580}/A_{510}, respectively.

$$y = 0.2911e^{0.1583x}, R^2 = 0.9791 \qquad (11)$$

Similar exponential calibration curves were also found in anthocyanins extracted from purple sweet potato (PSP) and film containing PSP anthocyanins.[39] The exponential calibration curve between pH and A_{580}/A_{510} for the GGG-RRA film indicated that RRA maintained good chemical activity in the GGG film. The visible color changes of GGG-RRA film toward pH change implied it was capable of indicating pH-related food quality.

3.2. Microstructure of the films. The SEM images showed that GGG film had a highly compact and dense appearance of cross section (Fig. 2A). This indicated that gelatin and gellan gum had excellent compatibility with each other due to the intermolecular interaction. Similar homogeneous structure of composite G and GG film was also observed in a previous study.[40] When a low content of RRA (i.e. 5 mg/100 mL) was added into the GGG film, some small spindrift-like structures appeared and was uniformly distributed in the film (Fig. 2B). With the increase of RRA content, the GGG-RRA films showed obvious aggregation of spindrift-like structures and stratification (Fig. 2C and Fig. 2D). When a relatively high content of RRA was added, the GGG-RRA20 film in turn became more uniform than the GGG-RRA10 and GGG-RRA15 film even though the size of spindrift-like structures was larger (Fig. 2E). This phenomenon could be explained by the gelation process of both gelation and gellan gum. During the gelation formation of gelatin, junction zones were formed by small segments of two or three polypeptide chains reverting to the collagen triple helix-like structure.[41] It has been reported that the addition of phenolic compounds promote the formation of hydrogen bonds among the three helices.[42] For the gellan gum, the formation of gels was closely affected by the pH of the solution. As gellan gum is a linear anionic polysaccharide, the aggregation of gellan gum helices in water was impeded by the intermolecular repulsion between negatively charged carboxylic groups on the gellan gum, while this intermolecular repulsion can be weakened with the decrease of pH of the solution, resulting in an enhancement of junction zone formation.[43] In this study, RRA as a phenol compound could also contribute to the gelation of gelatin. At the same time, with the increase of the RRA content, the pH of the solution decreased, contributing the gelation of gellan gum. Therefore, more intermolecular cross-linking within gelatin molecules and gellan gum molecules were generated, leading to partial phase separation of gelatin and gellan gum. As shown in Fig. 2B-D, the continuous and compact phase with parallel-arranged long chains could largely comprise gelatin molecules, while the coarse phase could largely comprise gellan gum. However, when the RRA content was at a relatively high level (20 mg/100 mL), the phase separation between gelatin and gellan gum molecules in the GGG-RRA20 film was not as obvious as that in the GGG-RRA10 and

GGG-RRA15 films. This might be due to excessive RRA having a steric hindrance effect on the formation of crosslinks among gelatin and gellan gum chains.

3.3. Mechanical and barrier properties. TS represents the capacity of the films to withstand loads tending to elongate and EB expresses the capability of the films to resist changes of shape without crack formation. The TS and EB of the GGG and GGG-RRA films are shown in Fig. 3A. With the increase of RRA content, the TS and EB of the films both become higher, indicating improved coupling strength and ductility of the films. The changes in mechanical properties of the films could be explained by the intermolecular interaction of G and GG in the absence and presence of RRA. The higher TS of the films in the presence of RRA could be due to the enhanced cross-linking among G and GG chains, respectively, as mentioned in section 2.3. Generally, an improved TS of a film was accompanied by a sacrifice of EB. However, the EB of the GGG-RRA films also increased with the increase of RRA. This could be due to the layer structure of the GGG-RRA films that endowed them with better flexibility compared to the GGG film.

Fig. 3B shows the UV-vis transmission spectra and images (inset) of GGG and GGG-RRA films. Pure GGG film was colorless and had a transparency of over 80% in the visible range of 400-800 nm. The incorporation of RRA into GGG film resulted in an orange color which became deeper with the increase of RRA content. The barrier property of the film to UV light could be obtained from the spectra in the range of 200-400 nm. GGG film presented excellent barrier properties to UV light in the range of 200-245 nm where the corresponding transparencies were lower than 1%, similar to a previous gelatin film.[44] Moreover, the UV light barrier ability of the films were significantly enhanced with RRA, since the films with higher RRA content showed improved barrier ability over broader spectra ranges. GGG-RRA20 film presented strong barrier ability to UV light in the range of 200-360 nm. These results could be due to the fact that RRA as a phenolic compound is favorable for the adsorption of UV radiation.[45] The good UV light barrier properties of GGG-RRA films may be beneficial for food preservation because UV light is known to induce deleterious change, particularly lipid oxidation, in foods.[46]

Fig. 3C shows the effect of RRA on the WVP of GGG films. Pure GGG film had a WVP value of 2.83 $g{\cdot}mm{\cdot}m^{-2}{\cdot}kPa^{-1}{\cdot}h^{-1}$, which was several orders of magnitude higher than that of polyethylene (PE) and poly(vinylidene chloride) (PVDC) films.[47] The high WVP of GGG film could be due to the hydrophilic nature of gelatin and gellan gum. With the increase of RRA content, the WVP of the films presented a first decline followed by a rise. For GGG-RRA10 film, the WVP was 1.25 $g{\cdot}mm{\cdot}m^{-2}{\cdot}kPa^{-1}{\cdot}h^{-1}$, which was lower than a half of the WVP value of the GGG film. As the RRA content increased to 20 mg/ 100 mL, the GGG-RRA20 film showed a comparable WVP (3.17 $g{\cdot}mm{\cdot}m^{-2}{\cdot}kPa^{-1}{\cdot}h^{-1}$) to the GGG film. The permeability of a film largely depends on its chemical structure, morphology and hydrophilicity, regardless of the environment conditions. The initial decrease of WVP of films with the increase of RRA content to 10 mg/ 100 mL could be due to anthocyanin enhancement of the interactions of both gelatin and gellan gum molecules, lowering the amount of gelatin and gellan gum molecules needed to form hydrophilic bonding with water and subsequently leading to a decrease in the affinity of the films towards water. Meanwhile, anthocyanins as phenolic components could form mainly non-covalent hydrophobic interactions with gelatin and gellan gum[48] and thus reduce the hydrophilicity of the films. However, a significant increase of WVP of the film was observed from the GGG-RRA15 and GGG-RRA20 films. This may be due to the high hydrophilicity of anthocyanins that made the film easier to absorb water when RRA content was too high. Hence, the results indicated that addition of a relatively low content of RRA in the GGG film beneficially lowered its mainly consequently reducing the water evaporation of packaged foods.

The GGG film had an oxygen permeability (OP) of 10.05 $cm^3 \cdot \mu m \cdot m^{-2} \cdot d^{-1} \cdot kpa^{-1}$ (Fig. 3D), which was much lower than low density polyethylene (LDPE) (1900 $cm^3 \cdot \mu m \cdot m^{-2} \cdot d^{-1} \cdot kPa^{-1}$) and higher than poly(vinylidene chloride) (PVDC) (0.1–3 $cm^3 \cdot \mu m \cdot m^{-2} \cdot d^{-1} \cdot kPa$) and ethylene-vinyl alcohol copolymers (EVOH) (0.77 $cm^3 \cdot \mu m \cdot m^{-2} \cdot d^{-1} \cdot kPa^{-1}$), but comparable to polyvinyl chloride (PVC) (20–80 $cm^3 \cdot \mu m \cdot m^{-2} \cdot d^{-1} \cdot kPa$)[49]. The increase of RRA content, caused the OP value of GGG-RRA films to slightly decrease to 6.33×10^{-2} $cm^3 \cdot \mu m \cdot m^{-2} \cdot d^{-1} \cdot kpa^{-1}$ (GGG-RRA20 film). The OP of the films was closely related to the diffusion path of oxygen within the film. The decrease of OP resulting from the increase in RRA content could be due to that the stronger crosslinking of gelatin and gellan gum leading to a reduction of the free volume for oxygen to pass through the films. The low OP of the GGG-RRA films may reduce the oxidation content of packaged foods.

3.4. Electrochemical writing on GGG-RRA film. In order to write information on the films using the electrochemical method, a hydrogel needed to be firstly fabricated. In this study, a firm gel with a good toughness was facilely formed after the GGG-RRA solution was cooled down without further treatment (Fig. 4A), attributed to the good gelation ability of gelatin and gellan gum. It is well known that the color of anthocyanins is dependent on pH condition[50], so the principle of electrochemical writing on the hydrogel can be expressed as in scheme 1. When the Pt needle was connected to the anode of the electrochemical workstation, a localized low pH condition was generated in the hydrogel due to the anodic water electrolysis reaction (equation 12) so that anthocyanins turned to acid color (orange red). On the contrary, when the Pt needle was connected to the cathode of the electrochemical workstation, a localized high pH condition was generated in the hydrogel due to the cathodic water electrolysis reaction (equation 13) and therefore anthocyanins turned to basic color (yellow).

$$2H_2O - 4e^- = 4H^+ + O_2 \uparrow \tag{12}$$

$$4H_2O + 4e^- = 4OH^- + 2H_2 \uparrow \tag{13}$$

The movement of the Pt needle along the horizontal plane was controlled by a mechanical arm to produce desired patterns. After being written on the hydrogels, the patterns were preserved by immediately drying the hydrogels to films. Apart from the current direction, the current magnitude could also make the color of the patterns different. When the current increased from 1 to 6 mA, the pattern “1” turned more acid (Fig. 4B) or basic colors (Fig. 4C). This was because a greater current led to more intense water electrolysis reaction and thus a greater acid or basic condition. Accordingly, multicolor patterns could be written on one film by tuning the current direction and magnitude. As shown in Fig. 4D and 4E, the flower with orange red petals and green calyces, and the apple with orange red fruit and yellow leaves were respectively drawn on individual films.

3.5. Color stability and gas sensing ability. The self-stability of the films and the written patterns are of great importance for the practical application of the films. Fig. 5A shows the images of the GGG-RRA10 film with red and yellow patterns stored at 75% for 30 d at 4, 25 and 37 °C. The color of the film and patterns gradually faded during storage. Especially at a higher temperature (37 °C), the film obviously turned less red and the patterns seriously discolored after 30 d. To describe the degree of discoloration, the relative color change (S) of the film and patterns was tested and shown in Fig. 5B. The S values of films and patterns increased slightly overall. In contrast, the S values were higher at a higher temperature for both the film and the patterns. At a certain temperature, the S values of the yellow pattern were higher than that of the red pattern followed by the film, indicating than the film had greater color stability than the red pattern and then the yellow pattern. Generally, the anthocyanins were more stable at lower pH.[51] The reason why the red pattern was less stable than the film remained unclear.

Before the film was employed as a gas sensor in the packaging system, its sensing ability to acid and basic gas were investigated. As shown in Fig. 5C and 5D, the GGG-RRA film gradually turned to redder after exposure to acetic acid gas, and turned to green after exposed to ammonia gas. This result suggested that the GGG-RRA film could be used to indicate the food spoilage when either acid or basic gases were the dominant volatile gases. As for the written patterns on the film, the red triangle maintained its original color in response to acetic acid (Fig. 5C) but gradually faded in response to ammonia (Fig. 6D). At the same time, the yellow triangle maintained yellow in response to ammonia (Fig. 6D) while gradually fading in response to acetic acid (Fig. 6C). Hence, to save the written information on the film, the films with red color patterns and yellow patterns could be used to indicate food spoilage during which acid gases and basic were the main volatile gases, respectively.

3.6. Application of films for indicating milk and fish spoilage. In this study, the GGG-RRA10 film was selected to indicate food quality, considering the effect of the anthocyanins concentration on the color visibility and gas sensitivity of the films discussed in our previous study.[12] The GGG-RRA10 films with red pattern “F” and yellow pattern “F” were used to monitor milk and fish spoilage, respectively. As shown in Fig. S1, the films were fixed on the lid to cover the hole that worked as the detection window through which the volatile gases generated from milk and fish diffused to contact with the film and make a color change of the film. In this way, the water vapor inside of the dishes could permeate through the film to the external environment to reduce the film swelling that might cause anthocyanins to leach from the film.

Fig. 6A shows the color change of the GGG-RRA10 film during the milk spoilage. With the increase of time, the film turned to be redder. The color change could also be seen from the color parameters, namely red (R), green (G) and blue (B). As shown in Fig. 6B, the R value increased from 232 to 253, indicating a deeper red color, while G and B value did not significantly change. The color change of the film implied that acid volatile gases were generated during the milk spoilage. Similar phenomena were also observed in a previous study.[13] This was largely due to the generation of organic acids during anaerobic respiration of anaerobic bacteria or facultative anaerobic bacteria under hypoxic or anaerobic condition. It is worth mentioning that the low OP of GGG-RRA10 film might contribute to a hypoxic condition for the anaerobic respiration of spoilage bacteria. The acidity of the milk was an important index to evaluate the freshness of milk. A higher acidity value indicated a larger amount of acid components and therefore an inferior freshness. As shown in Fig. 6B, the acidity of the milk increased from 14.78 to 25.67 °T after a 48 h storage at 25 °C. According to Chinese standard (GB 19645-2010), the acidity value of pasteurized milk should be under 18 °T to ensure quality. In this study, the acidity of the reached to

18 °T at nearly 25 h, while at this point the R value of the film was nearly 240. This implied that if the R value of the film was higher than 240, the milk sample should not be consumed.

Fig. 6C shows the color change of the GGG-RRA10 film during the spoilage of black carp. The film gradually turned from initial orange red to green (4 d) and then yellow green (8 d). Accordingly, the color parameter R decreased, and G increased from 0 d to the 4 d (Fig. 6D). However, the R and G value did not dramatically change after 4 d. Meanwhile, the B value decreased over time from initial an 144 to final 18, indicating a deeper yellow color (the complementary color of blue). Hence, the B value could be used as a characteristic parameter for the color change of the film. The color change of the film could be mainly induced by the volatile basic gases, such as ammonia, trimethylamine and dimethylamine, generated from the black carp. Fig. 6D shows the TVB-N content of the black carp. It rose from 4.74 mg/100g at 0 d to 53.71 mg/100g at 9 d at 4 °C. The generation of TVB-N was due to the decomposition of proteins by bacteria and enzymes. According to Chinese Standard (GB 2733-2015), the rejection limit of TVB-N level for black carp is 20 mg/100 g. In this study, the TVB-N value rose to 20 mg/100 g at nearly 5.5 d, when the B value of the film was around 87. This implied that if the B value of the film was lower than 87, then the fish sample should not be consumed.

For the written patterns “F” on the GGG-RRA10 films that were used for either milk or fish spoilage, as expect, they retained a clear color and shape (Fig. 6A and 6C). As can be seen from the Fig. S2A, R, G, and B values of the red “F” did not obviously change, indicating a good color stability. Although the B value of the yellow “F” significantly decreased (Fig. S2B), the pattern “F” still kept a bright yellow color because of the weak fluctuation of R and G values. Hence, the GGG-RRA film combined with written pattern could be used to indicate the milk and fish spoilage.

As mentioned above, when the GGG-RRA-10 film was used to indicate the milk and fish spoilage, the film showed visible color changes while the written patterns on the film maintained good shapes and colors. As the GGG-RRA films were made from degradable and edible biomaterials, and the patterns were in situ drawn on the films by using electrochemical method without the need of inks, they should have a great potential for practical application in intelligent food packaging.

ACKNOWLEDGMENT

The authors gratefully acknowledge the financial support provided by the Postgraduate Research & Practice Innovation Program of Jiangsu Province (KYCX17_1798), the National Science and Technology Support Program (2015BAD17B04), the National Key Research and Development Program of China (2016YFD0401104), the National Natural Science Foundation of China (31671844, 31601543), China Postdoctoral Science Foundation (2013M540422, 2014T70483, 2016M590422), the Natural Science Foundation of Jiangsu Province (BK20160506, BE2016306), International Science and Technology Cooperation Project of Jiangsu Province (BZ2016013), Suzhou Science and Technology Project (SNG201503) and Priority Academic Program Development of Jiangsu Higher Education Institutions (PAPD). We also would like to thank our colleagues in School of Food and Biological Engineering who provided assistance in this study.

NOTES

The authors declare no competing financial interest.

Supporting Information description

There were two figures in the supporting information file. Fig. S1 the photo of the deveice that was used to detect milk and fish spoilage. Fig. S2 was the change of the R, G, and B values of written patterns “F” on the GGG-RRA10 film used to monitor milk and fish spoilage.

REFERENCES

1. Realini, C. E.; Marcos, B., Active and intelligent packaging systems for a modern society. *Meat Sci.* **2014**, *98*, 404-19.

2. Ghaani, M.; Cozzolino, C. A.; Castelli, G.; Farris, S., An overview of the intelligent packaging technologies in the food sector. *Trends Food Sci. Technol.* **2016**, *51*, 1-11.

3. Pacquit, A.; Frisby, J.; Diamond, D.; Lau, K.; Farrell, A.; Quilty, B.; Diamond, D., Development of a smart packaging for the monitoring of fish spoilage. *Food Chem.* **2007**, *102*, 466-470.

4. Rukchon, C.; Nopwinyuwong, A.; Trevanich, S.; Jinkarn, T.; Suppakul, P., Development of a food spoilage indicator for monitoring freshness of skinless chicken breast. *Talanta* **2014**, *130*, 547-54.

5. Dainelli, D.; Gontard, N.; Spyropoulos, D.; Zondervan-van den Beuken, E.; Tobback, P., Active and intelligent food packaging: legal aspects and safety concerns. *Trends Food Sci. Technol.* **2008**, *19*, S103-S112.

6. Zhang, X.; Lu, S.; Chen, X., A visual pH sensing film using natural dyes from Bauhinia blakeana Dunn. *Sensors Actuators B: Chem.* **2014**, *198*, 268-273.

7. Luchese, C. L.; Abdalla, V. F.; Spada, J. C.; Tessaro, I. C., Evaluation of blueberry residue incorporated cassava starch film as pH indicator in different simulants and foodstuffs. *Food Hydrocoll.* **2018**, *82*, 209-218.

8. Pereira, V. A.; de Arruda, I. N. Q.; Stefani, R., Active chitosan/PVA films with anthocyanins from Brassica oleraceae (Red Cabbage) as Time–Temperature Indicators for application in intelligent food packaging. *Food Hydrocoll.* **2015**, *43*, 180-188.

9. Saliu, F.; Della Pergola, R., Carbon dioxide colorimetric indicators for food packaging application: Applicability of anthocyanin and poly-lysine mixtures. *Sensors Actuators B: Chem.* **2018**, *258*, 1117-1124.

10. Silva-Pereira, M. C.; Teixeira, J. A.; Pereira-Júnior, V. A.; Stefani, R., Chitosan/corn starch blend films with extract from Brassica oleraceae (red cabbage) as a visual indicator of fish deterioration. *LWT - Food Sci. Technol.* **2015**, *61*, 258-262.

11. Wei, Y.-C.; Cheng, C.-H.; Ho, Y.-C.; Tsai, M.-L.; Mi, F.-L., Active gellan gum/purple sweet potato composite films capable of monitoring pH variations. *Food Hydrocoll.* **2017**, *69*, 491-502.

12. Zhai, X.; Shi, J.; Zou, X.; Wang, S.; Jiang, C.; Zhang, J.; Huang, X.; Zhang, W.; Holmes, M., Novel colorimetric films based on starch/polyvinyl alcohol incorporated with roselle anthocyanins for fish freshness monitoring. *Food Hydrocoll.* **2017**, *69*, 308-317.

13. Ma, Q.; Wang, L., Preparation of a visual pH-sensing film based on tara gum incorporating cellulose and extracts from grape skins. *Sensors Actuators B: Chem.* **2016**, *235*, 401-407.

14. Ma, Q.; Ren, Y.; Gu, Z.; Wang, L., Developing an intelligent film containing Vitis amurensis husk extracts: The effects of pH value of the film-forming solution. *J. Clean. Prod.* **2017**, *166*, 851-859.

15. Kuswandi, B.; Jayus; Larasati, T. S.; Abdullah, A.; Heng, L. Y., Real-Time Monitoring of Shrimp Spoilage Using On-Package Sticker Sensor Based on Natural Dye of Curcumin. *Food Anal. Methods* **2011**, *5*, 881-889.

16. Ma, Q.; Du, L.; Wang, L., Tara gum/polyvinyl alcohol-based colorimetric NH3 indicator films incorporating curcumin for intelligent packaging. *Sensors Actuators B: Chem.* **2017**, *244*, 759-766.

17. Liu, J.; Wang, H.; Wang, P.; Guo, M.; Jiang, S.; Li, X.; Jiang, S., Films based on κ-carrageenan incorporated with curcumin for freshness monitoring. *Food Hydrocoll.* **2018**.

18. Musso, Y. S.; Salgado, P. R.; Mauri, A. N., Smart edible films based on gelatin and curcumin. *Food Hydrocoll.* **2017**, *66*, 8-15.

19. Otsuki, T.; Matsufuji, H.; Takeda, M.; Toyoda, M.; Goda, Y., Acylated anthocyanins from red radish (Raphanus sativus L.). *Phytochemistry* **2002**, *60*, 79-87.

20. Matsufuji, H.; Kido, H.; Misawa, H.; Yaguchi, J.; Otsuki, T.; Chino, M.; Takeda, M.; Yamagata, K., Stability to Light, Heat, and Hydrogen Peroxide at Different pH Values and DPPH Radical Scavenging Activity of Acylated Anthocyanins from Red Radish Extract. *J. Agric. Food. Chem.* **2007**, *55*, 3692-3701.

21. Park, N. I.; Xu, H.; Li, X.; Jang, I. H.; Park, S.; Ahn, G. H.; Lim, Y. P.; Kim, S. J.; Park, S. U., Anthocyanin Accumulation and Expression of Anthocyanin Biosynthetic Genes in Radish (Raphanus sativus). *J. Agric. Food. Chem.* **2011**, *59*, 6034-6039.

22. Martucci, J. F.; Accareddu, A. E. M.; Ruseckaite, R. A., Preparation and characterization of plasticized gelatin films cross-linked with low concentrations of Glutaraldehyde. *J. Mater. Sci.* **2012**, *47*, 3282-3292.

23. Guo, J.; Ge, L.; Li, X.; Mu, C.; Li, D., Periodate oxidation of xanthan gum and its crosslinking effects on gelatin-based edible films. *Food Hydrocoll.* **2014**, *39*, 243-250.

24. Boateng, J.; Burgos-Amador, R.; Okeke, O.; Pawar, H., Composite alginate and gelatin based bio-polymeric wafers containing silver sulfadiazine for wound healing. *Int. J. Biol. Macromol.* **2015**, *79*, 63-71.

25. Samp, M. A.; Iovanac, N. C.; Nolte, A. J., Sodium Alginate Toughening of Gelatin Hydrogels. *ACS Biomater. Sci. Eng.* **2017**, *3*.

26. Qiao, C.; Ma, X.; Zhang, J.; Yao, J., Molecular interactions in gelatin/chitosan composite films. *Food Chem.* **2017**, *235*, 45-50.

27. Zia, K. M.; Tabasum, S.; Khan, M. F.; Akram, N.; Akhter, N.; Noreen, A.; Zuber, M., Recent trends on gellan gum blends with natural and synthetic polymers: A review. *Int. J. Biol. Macromol.* **2018**, *109*, 1068-1087.

28. Ferris, C. J.; Gilmore, K. J.; Wallace, G. G.; Panhuis, M. I. H., Modified gellan gum hydrogels for tissue engineering applications. *Soft Matter* **2013**, *9*, 3705-3711.

29. Lee, K. Y.; Shim, J.; Lee, H. G., Mechanical properties of gellan and gelatin composite films. *Carbohydr. Polym.* **2004**, *56*, 251-254.

30. Xu, X.-J.; Fang, S.; Li, Y.-H.; Zhang, F.; Shao, Z.-P.; Zeng, Y.-T.; Chen, J.; Meng, Y.-C., Effects of low acyl and high acyl gellan gum on the thermal stability of purple sweet potato anthocyanins in the presence of ascorbic acid. *Food Hydrocoll.* **2018**.

31. Robert, T., “Green ink in all colors”—Printing ink from renewable resources. *Prog. Org. Coat.* **2015**, *78*, 287-292.

32. Aznar, M.; Domeño, C.; Nerín, C.; Bosetti, O., Set-off of non volatile compounds from printing inks in food packaging materials and the role of lacquers to avoid migration. *Dyes and Pigments* **2015**, *114*, 85-92.

33. Wang, H.; Qian, J.; Li, H.; Ding, F., Rheological characterization and simulation of chitosan-TiO2 edible ink for screen-printing. *Prog. Org. Coat.* **2018**, *120*, 19-27.

34. Wu, S.; Wang, W.; Yan, K.; Ding, F.; Shi, X.; Deng, H.; Du, Y., Electrochemical writing on edible polysaccharide films for intelligent food packaging. *Carbohydr. Polym.* **2018**, *186*, 236-242.

35. Wang, Z.; Li, Y.; Chen, L.; Xin, X.; Yuan, Q., A study of controlled uptake and release of anthocyanins by oxidized starch microgels. *J. Agric. Food. Chem.* **2013**, *61*, 5880-7.

36. Xiaowei, H.; Xiaobo, Z.; Jiewen, Z.; Jiyong, S.; Zhihua, L.; Tingting, S., Monitoring the biogenic amines in Chinese traditional salted pork in jelly (Yao-meat) by colorimetric sensor array based on nine natural pigments. *Int. J. Food Sci. Tech.* **2015**, *50*, 203-209.

37. Lixin, L.; Weizhou, Z.; Zhiye, L.; Yali, T., Development and Application of Time–temperature Indicators Used on Food during the Cold Chain Logistics. *Packag. Technol. Sci.* **2013**, *26*, 80-90.

38. Cai, J.; Chen, Q.; Wan, X.; Zhao, J., Determination of total volatile basic nitrogen (TVB-N) content and Warner-Bratzler shear force (WBSF) in pork using Fourier transform near infrared (FT-NIR) spectroscopy. *Food Chem.* **2011**, *126*, 1354-1360.

39. Choi, I.; Lee, J. Y.; Lacroix, M.; Han, J., Intelligent pH indicator film composed of agar/potato starch and anthocyanin extracts from purple sweet potato. *Food Chem.* **2017**, *218*, 122-128.

40. Pranoto, Y.; Lee, C. M.; Park, H. J., Characterizations of fish gelatin films added with gellan and κ-carrageenan. *LWT - Food Sci. Technol.* **2007**, *40*, 766-774.

41. Fonkwe, L. G.; Narsimhan, G.; Cha, A. S., Characterization of gelation time and texture of gelatin and gelatin–polysaccharide mixed gels. *Food Hydrocoll.* **2003**, *17*, 871-883.

42. Jin, W.; Shih‐Chien, C.; M., P. E.; K., K. T., Effects of phenolic compounds on gelation behavior of gelatin gels. *J. Polym. Sci., Part A: Polym. Chem.* **2001**, *39*, 224-231.

43. Picone, C. S. F.; Cunha, R. L., Influence of pH on formation and properties of gellan gels. *Carbohydr. Polym.* **2011**, *84*, 662-668.

44. Jiang, Y.; Li, Y.; Zhi, C.; Leng, X., Study of the Physical Properties of Whey Protein Isolate and Gelatin Composite Films. *J. Agric. Food. Chem.* **2010**, *58*, 5100-5108.

45. Bitencourt, C. M.; Fávaro-Trindade, C. S.; Sobral, P. J. A.; Carvalho, R. A., Gelatin-based films additivated with curcuma ethanol extract: Antioxidant activity and physical properties of films. *Food Hydrocoll.* **2014**, *40*, 145-152.

46. Prodpran, T.; Benjakul, S.; Phatcharat, S., Effect of phenolic compounds on protein cross-linking and properties of film from fish myofibrillar protein. *Int. J. Biol. Macromol.* **2012**, *51*, 774-782.

47. Parris, N.; Coffin, D. R.; RF, J.; H, P., Composition factors affecting the water vapor permeability and tensile properties of hydrophilic films. *J. Agric. Food Chem.* **1997**, *45*, 1596-1599.

48. Jakobek, L., Interactions of polyphenols with carbohydrates, lipids and proteins. *Food Chem.* **2015**, *175*, 556-567.

49. Garusinghe, U. M.; Varanasi, S.; Raghuwanshi, V. S.; Garnier, G.; Batchelor, W., Nanocellulose-montmorillonite composites of low water vapour permeability. *Colloids Surf. Physicochem. Eng. Aspects* **2018**, *540*, 233-241.

50. Castañeda-Ovando, A.; Pacheco-Hernández, M. d. L.; Páez-Hernández, M. E.; Rodríguez, J. A.; Galán-Vidal, C. A., Chemical studies of anthocyanins: A review. *Food Chem.* **2009**, *113*, 859-871.

51. Torskangerpoll, K.; Andersen, O. M., Colour stability of anthocyanins in aqueous solutions at various pH values. *Food Chem.* **2005**, *89*, 427-440.

Figure captions

Fig. 1. The color (A) and UV-vis spectra (B) of RRA anthocyanins extract solution at pH 2-12, and the color (C) and UV-vis spectra (D) of GGG-RRA10 film at pH 2-12. Insets of (B) and (D) were the change of A_{580}/A_{510} of the RRA solution and GGG-RRA10 film with the change of pH, respectively.

Fig. 2. The SEM images of cross sections of GGG (A), GGG-RRA5 (B), GGG-RRA10 (C), GGG-RRA15 (D) and GGG-RRA20 film (E).

Fig. 3. The mechanical properties (A), transparencies (B), WVP (C) and OP (D) of the GGG and GGG-RRA films.

Scheme 1. The principle of electrochemical writing on GGG-RRA film.

Fig. 4. The photo of GGG-RRA10 hydrogel (A); the images of pattern "1" at different current magnitude when the Pt needle was connected with the anode (B) and cathode (C) of the electrochemical workstation; the images of multicolor pattern flower (D) and apple (E) written on the film.

Fig. 5. Images (A) and the corrsponding S values (B) of the GGG-RRA10 film with written patterns stored at 4, 25 and 37 °C for 30 days; the color response of the GGG-RRA10 film with written patterns towards acetic acid (C) and ammonia gas (D).

Fig. 6. Images of GGG-RRA10 film with red pattern "F" when used to monitor the milk spoilage at 25 °C (A), and the corresponding R, G, B values changes of the film and the acidity change of the milk (B); Images of GGG-RRA10 film with yellow pattern "F" when used to monitor the black carp spoilage at 4 °C (C), and the corresponding R, G, B value changes of the film and the TVB-N content changes of the black carp (D).

Figure 1.

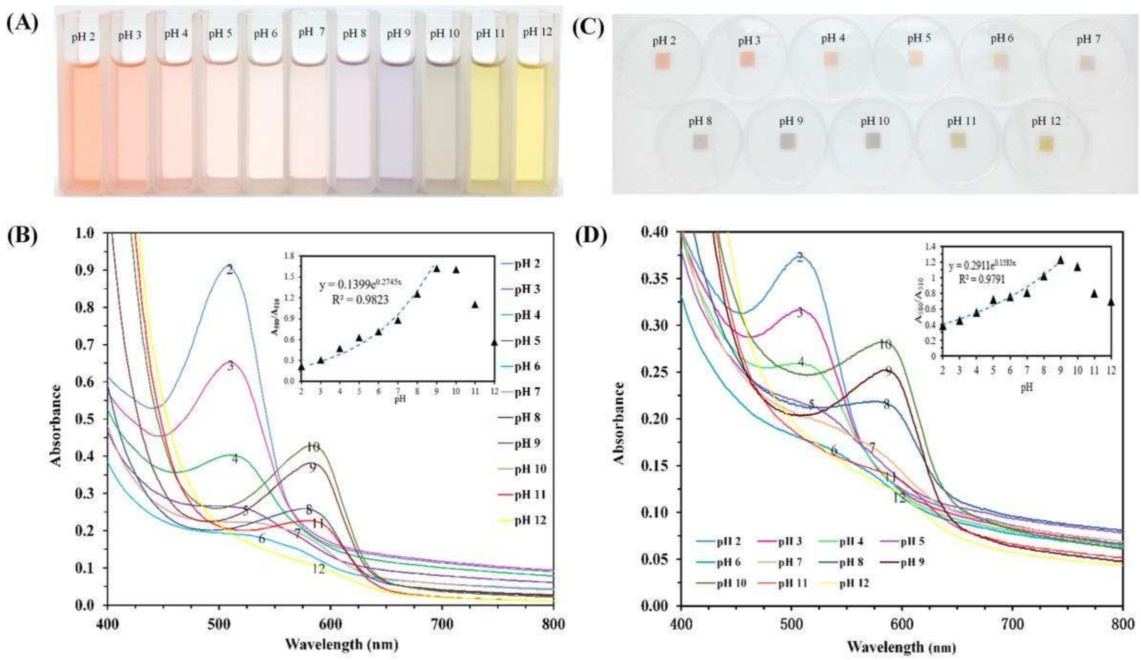
(A)
pH 2
pH 3
pH 4
pH 5
pH 6
pH 7
pH 8
pH 9
pH 10
pH 11
pH 12
(C)
pH 2
pH 3
pH 4
pH 5
pH 6
pH 7
pH 8
pH 9
pH 10
pH 11
pH 12
(B)
Absorbance
Wavelength (nm)
1.0
0.9
0.8
0.7
0.6
0.5
0.4
0.3
0.2
0.1
0.0
400
500
600
700
800
2
3
4
5
6
7
8
9
10
11
12
y = 0.1399e^0.2745x
R² = 0.9823
A580/A510
pH
pH 2
pH 3
pH 4
pH 5
pH 6
pH 7
pH 8
pH 9
pH 10
pH 11
pH 12
(D)
Absorbance
Wavelength (nm)
0.40
0.35
0.30
0.25
0.20
0.15
0.10
0.05
0.00
400
500
600
700
800
y = 0.2911e^0.1583x
R² = 0.9791
A580/A510
pH
pH 2
pH 3
pH 4
pH 5
pH 6
pH 7
pH 8
pH 9
pH 10
pH 11
pH 12

Figure 2.

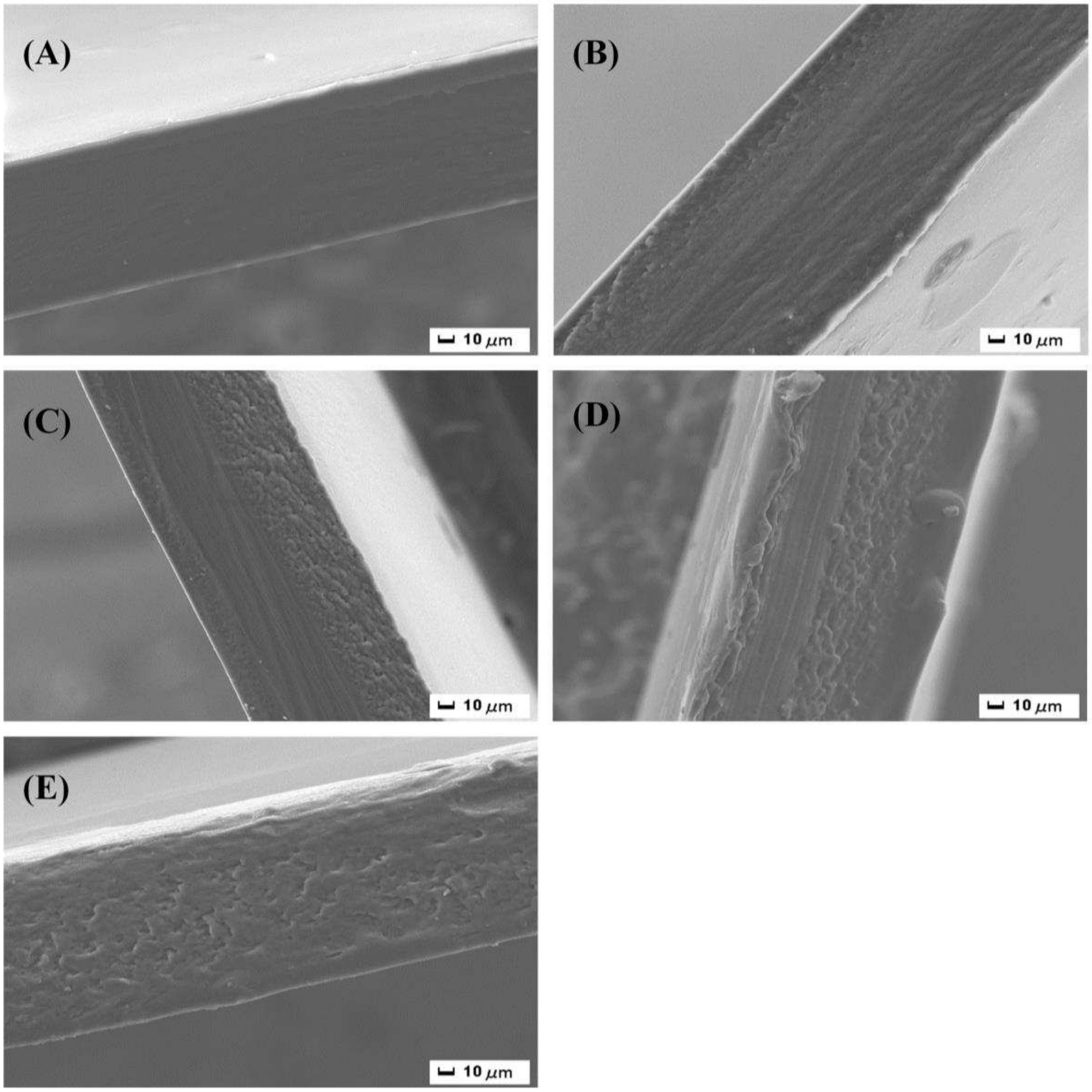

Figure 3.

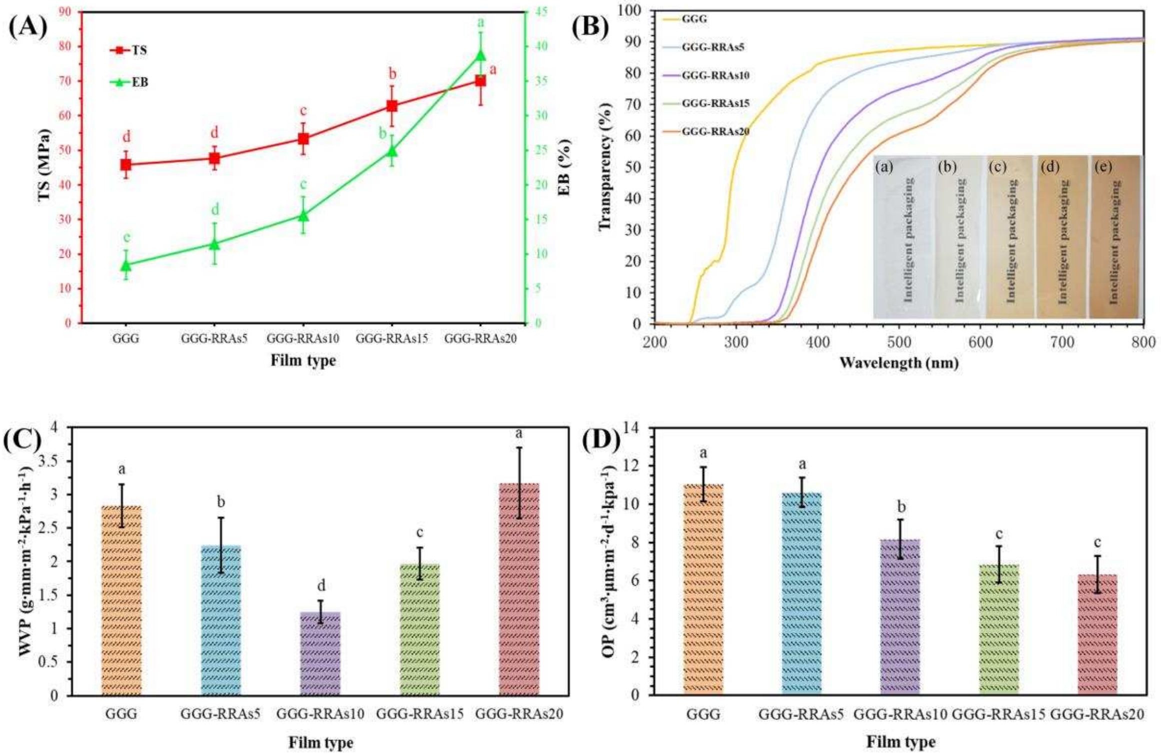
(A)
TS
EB
TS (MPa)
EB (%)
Film type
GGG
GGG-RRAs5
GGG-RRAs10
GGG-RRAs15
GGG-RRAs20
(B)
GGG
GGG-RRAs5
GGG-RRAs10
GGG-RRAs15
GGG-RRAs20
Transparency (%)
Wavelength (nm)
(a)
(b)
(c)
(d)
(e)
Intelligent packaging
(C)
WVP (g·mm·m-2·kPa-1·h-1)
Film type
(D)
OP (cm3·μm·m-2·d-1·kpa-1)
Film type

Scheme 1.

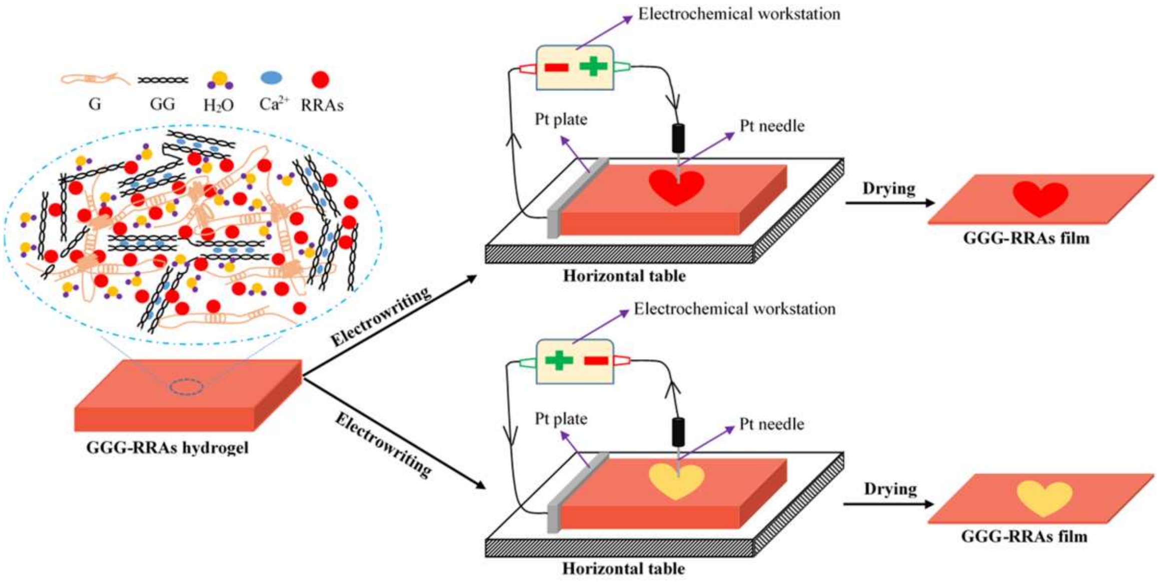
G
GG
H_2O
Ca^{2+}
RRAs
GGG-RRAs hydrogel
Electrowriting
Electrochemical workstation
Pt plate
Pt needle
Horizontal table
Drying
GGG-RRAs film
Electrowriting
Electrochemical workstation
Pt plate
Pt needle
Horizontal table
Drying
GGG-RRAs film

Figure 4.

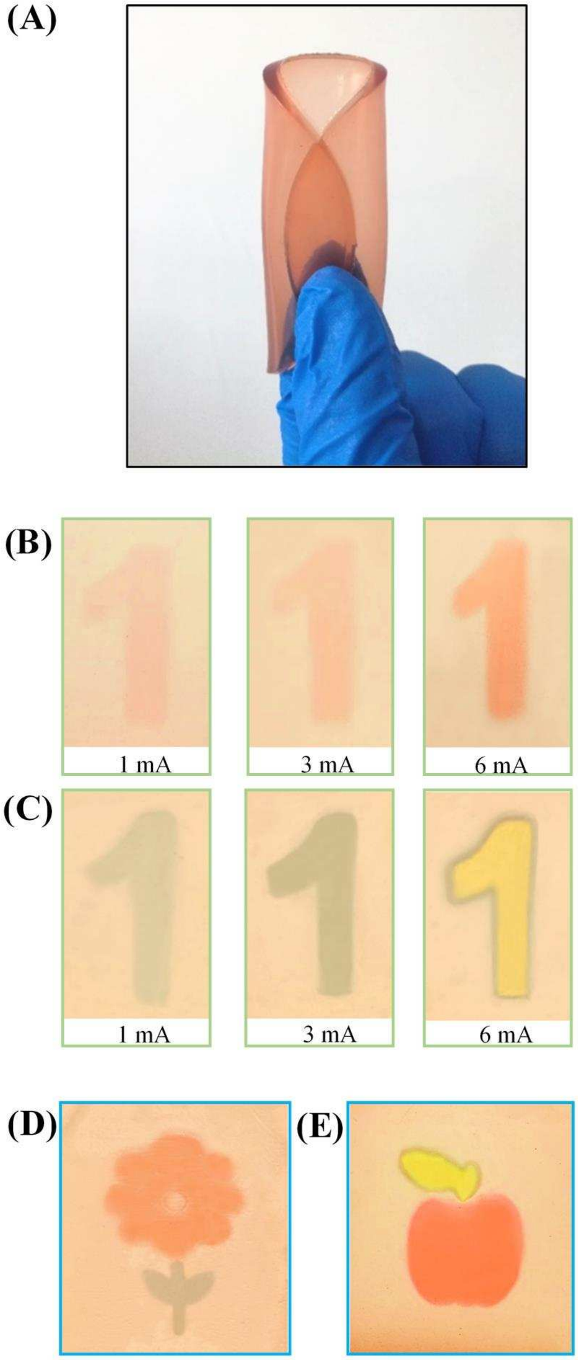

Figure 5.

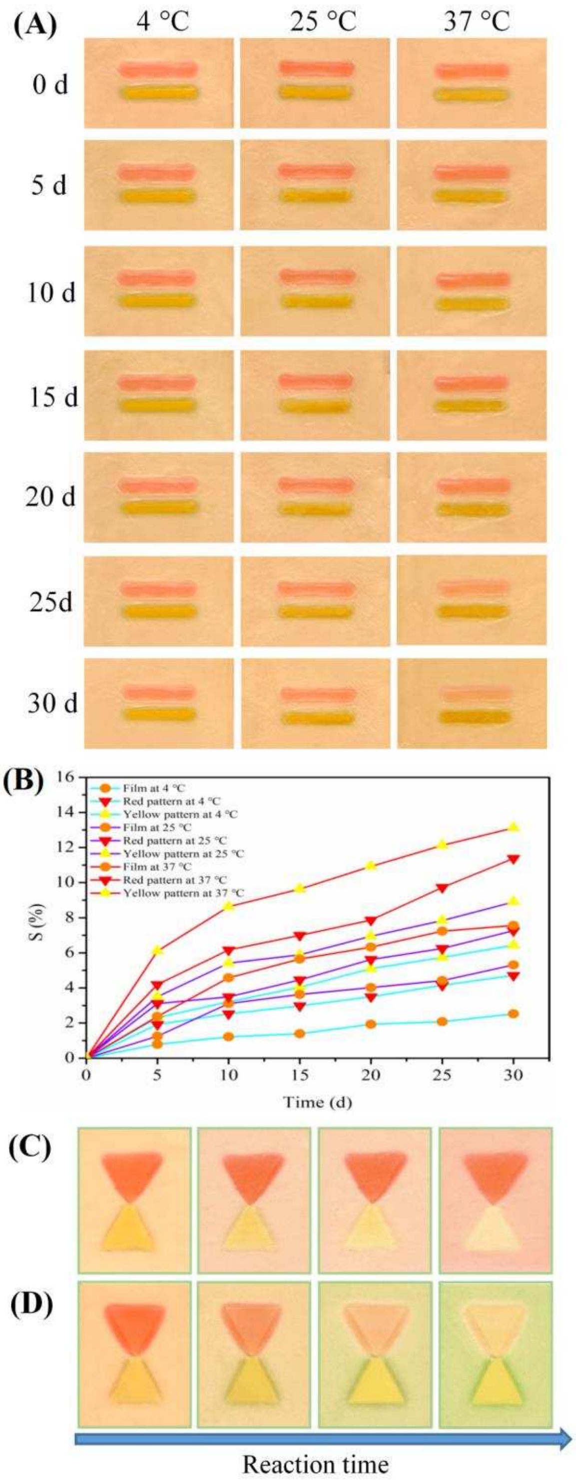
(A)
4 °C
25 °C
37 °C
0 d
5 d
10 d
15 d
20 d
25d
30 d
(B)
Film at 4 °C
Red pattern at 4 °C
Yellow pattern at 4 °C
Film at 25 °C
Red pattern at 25 °C
Yellow pattern at 25 °C
Film at 37 °C
Red pattern at 37 °C
Yellow pattern at 37 °C
S (%)
0
2
4
6
8
10
12
14
16
0
5
10
15
20
25
30
Time (d)
(C)
(D)
Reaction time

Figure 6.

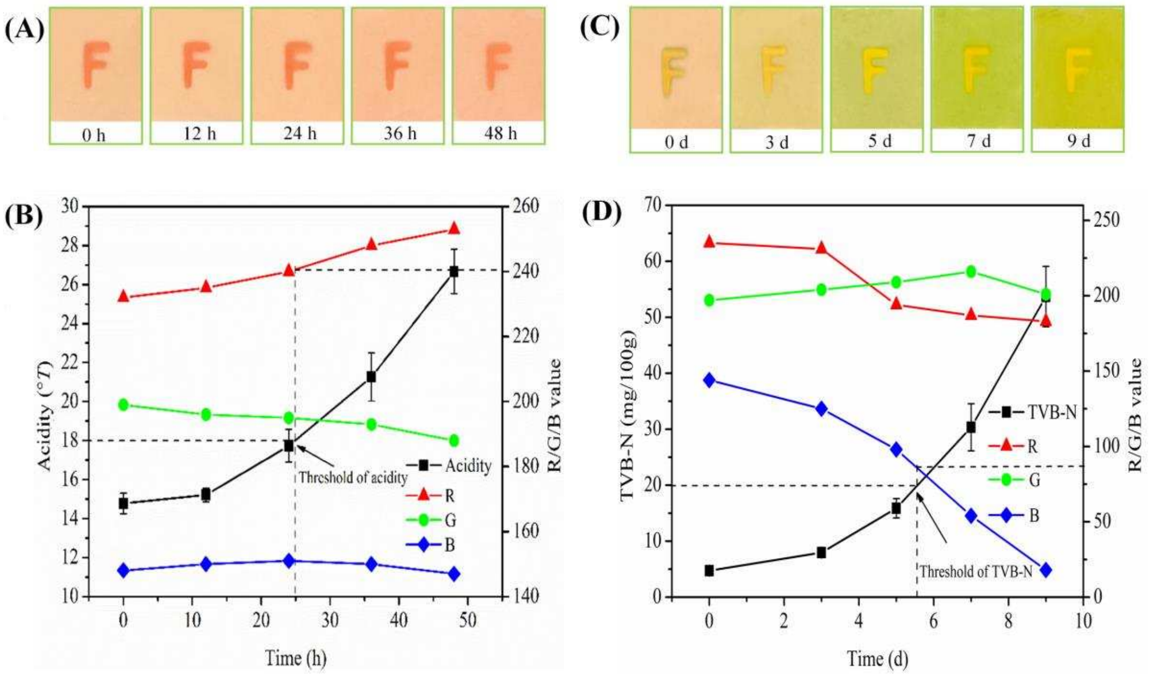
(A)
0 h
12 h
24 h
36 h
48 h
(C)
0 d
3 d
5 d
7 d
9 d
(B)
Acidity (°T)
R/G/B value
Time (h)
Acidity
R
G
B
Threshold of acidity
30
28
26
24
22
20
18
16
14
12
10
260
240
220
200
180
160
140
0
10
20
30
40
50
(D)
TVB-N (mg/100g)
R/G/B value
Time (d)
TVB-N
R
G
B
Threshold of TVB-N
70
60
50
40
30
20
10
0
250
200
150
100
50
0
0
2
4
6
8
10